Research Article | Vol. 26, No. 26 | 24 Dec 2018 | OPTICS EXPRESS 34094
Optics EXPRESS

A semi-analytical model for estimating total suspended matter in highly turbid waters

YIBO ZHANG,[1,2,3] KUN SHI,[1,2,4,*] YUNLIN ZHANG,[1,2] MAX J. MORENO-MADRINAN,[3] YUAN LI,[5] AND NA LI[1]

[1]State Key Laboratory of Lake Science and Environment, Nanjing Institute of Geography and Limnology, Chinese Academy of Sciences, Nanjing 210008, China
[2]University of Chinese Academy of Sciences, Beijing 100049, China
[3]Department of Environmental Health, Fairbanks School of Public Health at Indiana University, IUPUI, Indianapolis, IN 46202, USA
[4]CAS Center for Excellence in Tibetan Plateau Earth Sciences, Beijing 100101, China
[5]School of Tourism and City Management, Zhejiang Gongshang University, Hangzhou 310018, China
*kshi@niglas.ac.cn

Abstract: Total suspended matter (TSM) is related to water quality. High TSM concentrations limit underwater light availability, thus affecting the primary productivity of aquatic ecosystems. Accurate estimation of TSM concentrations in various waters with remote sensing technology is particularly challenging, as the concentrations and optical properties vary greatly among different waters. In this research, a semi-analytical model was established for Hangzhou Bay and Lake Taihu for estimating TSM concentration. The model construction proceeded in two steps. 1) Two indices of the model were calculated by deriving absorption and backscattering coefficients of suspended matter ($a_p(\lambda)$ and $b_{bp}(\lambda)$) from the reflectance signal using a semi-analytical method. 2) The two indices were then weighted to derive TSM. The performance of the proposed model was tested using *in situ* reflectance and Geostationary Ocean Color Imager (GOCI) data. The derived TSM based on *in situ* reflectance and GOCI images both corresponded well with the *in situ* TSM with low mean relative error (32%, 41%), root mean square error (20.1 mg/L, 43.1 mg/L), and normalized root mean square error (33%, 55%). The model was further used for the slightly turbid Xin'anjiang Reservoir to demonstrate its applicability to derive $a_p(\lambda)$ and $b_{bp}(\lambda)$ in other water types. The results indicated that the form $R_{rs}^{-1}(\lambda_1) - R_{rs}^{-1}(\lambda_2)$ could minimize the effect of CDOM absorption in deriving $a_p(\lambda)$ from the total absorption. The model exploited the different relationships between TSM concentration and multiband reflectance, thus improving the performance and application range in deriving TSM.

1. Introduction

Total suspended sediment (TSM) is closely related to water transparency and other water quality parameters. TSM is mainly composed of fine and medium silt, which can be easily resuspended and transported to the water surface [1]. High TSM concentrations in shallow lakes can be partly attributed to sediment resuspension by wind waves and runoff discharge [2–4]. In coastal water, terrestrial inputs and tidal action predominantly cause high TSM in the water column [1,5,6]. High TSM concentrations limit the light penetration into the underwater environment, thereby affecting the primary productivity of aquatic ecosystem [5,6]. In addition, high TSM concentrations are accompanied by high levels of nutrients, phosphorus, micropollutants, heavy metals, and other pollutants, which negatively impact human and ecosystem health.

Obtaining TSM concentrations with fine temporal and spatial resolution is important for evaluating water quality and associated environmental functions. Traditional *in situ* TSM measurements can be expensive and time-consuming. In addition, it is challenging to obtain

#349794 https://doi.org/10.1364/OE.26.034094
Journal © 2018 Received 1 Nov 2018; revised 11 Dec 2018; accepted 12 Dec 2018; published 14 Dec 2018

Optics EXPRESS

TSM concentrations simultaneously over a large scale or monitor long-term processes in aquic environments [4]. Overcoming this problem could be accomplished by an increase in the use of satellite remote sensing.

The fundamental theory of the use of remote sensing to derive TSM concentrations is that the backscattering properties of TSM enhance the remote sensing signal, while the absorption properties reduce the signal. Both the absorption and backscattering coefficient of TSM are significantly elevated with increasing sediment, which makes it possible to construct relationships between TSM and the remote sensing signal. Over the past several decades, an increasing number of studies based on analytical, empirical and semi-analytical methods have mapped TSM concentrations with satellite data around the world [7–13]. The analytical models in these studies were based on strict theoretical derivation, which tends to be more applicable for different water types than empirical models. However, challenges or inaccuracies in obtaining initialization parameters limited the implementation of these models in a wider range of conditions [7]. The empirical models were established based on statistical relationships between TSM concentrations and water reflectance or radiance in visible or near-infrared (NIR) wavelengths of a single band, band ratios, or multiple bands, and the band selection usually covaried with the optical properties of the water environment. For instance, the absorbing coefficient of pure water is significantly larger in the NIR region than in short visible regions. Therefore, the reflectance in the NIR region is suggested for estimating high TSM, which could ensure a sufficient reflectance signal in this region, while the less-absorbing portions in short visible wavelengths are more suitable for low TSM [14,15]. In addition to the choice of spectral bands, the band arithmetic also varies with water types from clear ocean water to highly turbid inland/coastal water. A single band model is accepted if an accurate water-leaving radiance or water surface reflectance can be derived from the raw image data [16]. The band ratio model can partly reduce skylight reflectance [17]. In addition, the effect of backscattering in deriving TSM from remote sensing reflectance could also be reduced by using an appropriate band ratio [18]. Multi-band models have demonstrated improved accuracy by cancelling spectrally covarying errors [19], even though they were usually used with either uncorrected at-sensor radiances or corrected remote sensing reflectance at coarser accuracy [20].

In addition to analytical and empirical models, semi-analytical methods are widely used to estimate TSM. Volpe, et al. [9] followed a theoretical approach to relate *in situ* measurements and satellite radiance observations for TSM estimation in a lagoon in Venice (Italy). Dekker, et al. [10] used an analytical model with *in situ* optical properties of particulate matter to assess the TSM variation in the southern Frisian lakes of the Netherlands. However, the most widely used form of the semi-analytical method is to derive the inherent optical properties (IOPs) of suspended matter (absorption and backscattering coefficient: $a_p(\lambda)$ and $b_{bp}(\lambda)$) from the water surface reflectance ($R_{rs}(\lambda)$) [21]. The relationship between $b_{bp}(\lambda)$ and $R_{rs}(\lambda)$ has been the subject of numerous studies [22–24]. In these studies, the optimal band is usually in the NIR region, where the absorption due to particulate and dissolved matter is assumed to be negligible. Therefore, the TSM is primarily derived from a single parameter, the total backscattering coefficient [16,25]. Similarly, if $a_p(\lambda)$ can be derived from $R_{rs}(\lambda)$, it can then be used for TSM retrieval [19,23]. Based on the radiative transfer theory, Lee, et al. [26] gave a theoretical explanation of $a_p(\lambda)$ and $b_{bp}(\lambda)$ and then established a quasi-analytical algorithm (QAA) for relating $a_p(\lambda)$ and $b_{bp}(\lambda)$ to multiband surface reflectance for ocean and coastal environments. Many subsequent works have presented applications of the QAA model in deriving $a_p(\lambda)$ as well as $b_{bp}(\lambda)$ from remote sensing reflectance and, consequently, for estimating the surface TSM concentration in different water types [11–13]. The semi-analytical methods allow insights on the process themselves and provide a representation of the current water condition that is consistent with the governing physical processes [9,10]. However, these methods need initialization parameters as input, which is challenging to obtain from current instruments due to their insufficient angular and spectral ranges. In

Optics EXPRESS

addition, a robust inversion model for a wide range of TSM concentrations has not been developed [19].

Lake Taihu and Hangzhou Bay, which are situated in the most heavily urbanized area in China, provide important water and fishery resources for the surrounding residents [27,28]. Effective monitoring and assessment of the water environment are therefore essential for ensuring water ecological security. In Lake Taihu, the water body is subject to frequent sediment resuspension from wind waves [27]. In Hangzhou Bay, sediment resuspension is mainly caused by the force of regular tides [28]. Both Lake Taihu and Hangzhou Bay are characterized by high turbidity and drastic variation, which has a profound impact on lake and bay ecosystems. Therefore, the capability to access high-frequency and large-scale observations is of great practical interest for environmentalists and ecologists. Current polar-orbiting satellites can only observe ground once a day, which is far below demand of hourly observation. Compared with these polar-orbiting satellites, the high revisit frequency of the Geostationary Ocean Color Imager (GOCI) will greatly improve our ability to monitor TSM dynamics in these regions.

Therefore, our aims in this study were to (1) characterize the water quality and spectral characteristics of Lake Taihu and Hangzhou Bay; (2) calibrate and validate a general semi-analytical model of TSM estimation ultimately applied to GOCI images; (3) examine the feasibility of using this model for other types of waters by applying it to the slightly turbid Xin'anjiang Reservoir; and (4) compare the superiority of this model in deriving the absorption and backscattering coefficients of TSM with existing models.

2. Data and methods

2.1 Study area

In situ measurements (Table 1) were collected from the highly turbid inland Lake Taihu (30°50′-31°40′ N and 119°50′-120°40′E) and highly turbid coastal waters of Hangzhou Bay (30°20′-30°40′N; 121°00′-121°20′ E) on the southeast coast of China (Fig. 1). Lake Taihu is located downstream of the Yangtze River and provides water resources for more than 10 million people in three cities (Wuxi City, Suzhou City, Huzhou City, and Shanghai). Lake Taihu is a turbid, shallow lake with long-term average Secchi depths of 0.35 m in the north and 0.45 m in the south [27]. The mean water depth of Lake Taihu is approximate 1.9 m, and the maximum depth is approximately 2.6 m at a water level of 3.0 m [27]. In Meiliang Bay and the open area of the lake, wind speeds often exceed 5 m/s, causing significant sediment resuspension and drastic spatial-temporal variation [27]. Hangzhou Bay is the largest bay on the southeastern coast of China and adjoins the mouth of the Yangtze River [29]. Two large rivers, the Yangtze River and the Qiantang River, flow into Hangzhou Bay. The multiannual mean water discharge from Yangtze River and Qiantang River are 900 km^3/yr and 42 km^3/yr, respectively, with an average sediment discharge of 5×10^8 t/yr and 8×10^6 t/yr [28]. In addition, Hangzhou Bay is characterized by strong tidal currents, with a maximal flood velocity of more than 3.0 m/s and an average amplitude of 3~4 m at the mouth of the bay [28]. Three field campaigns in Lake Taihu were conducted in August 2013, August 2014, and April 2015. One field campaign in Hangzhou Bay was conducted in July 2017. The water parameter measurements included TSM, organic suspended matter (OSM), and inorganic suspended matter (ISM) concentrations and the absorption of TSM ($a_p(\lambda)$) and chromophoric dissolved organic matter (CDOM) ($a_{CDOM}(\lambda)$).

2.2 Samples and $R_{rs}(\lambda)$ collection

Water samples were collected at 0.5 m under the water surface immediately after water spectral measurement. All samples were stored in a dark and cool container for transport to the laboratory.

Optics EXPRESS

Each water sample (100–500 ml determined by water turbidity) was filtered with a 0.7-μm Whatman GF/F filter. The filter was pre-combusted at a constant temperature of 550 °C for 4 h to remove organic matter. The filters were then dried at a constant temperature of 105 °C for 4 h to obtain TSM with an accuracy of 0.01 mg. The filters were re-combusted to obtain ISM and OSM.

Each water sample was filtered with a Whatman GF/F filter before measuring the absorption spectra between 350 and 800 nm with 1-nm intervals by using a Shimadzu UV-2500 PC UV-Vis spectrophotometer. The details of the measurement and calculation of $a_p(\lambda)$ using quantitative filter technique method were presented in a previous study [30].

Water samples were filtered prior to CDOM absorption analysis using pre-combusted 0.7-μm Whatman GF/F filters and 0.22-μm Millipore cellulose membranes. The absorption spectra of CDOM between 240 and 800 nm with an interval of 1 nm were obtained using a Shimadzu UV-2500 PC UV-Vis spectrophotometer [31]. The absorption coefficient of CDOM at 254 nm, $a_{CDOM}(254)$, is used in this study as a proxy of CDOM concentration. Many previous studies have used $a_{CDOM}(254)$ to demonstrate the spatial-temporal distribution of CDOM concentrations in different water bodies [31,32].

Water spectra (total downwelling and upwelling radiance) were measured between 10:00 and 15:00 Beijing time (China) on sunny days by using an Analytical Spectral Devices instrument (ASD, Inc., Boulder, CO). The water spectra were collected at an azimuth angle of 90–135° and a nadir view angle of 30–45°. After that, the spectrometer was adjusted upwards to 90–120° to obtain the spectra of the downwelling sky radiance. Finally, downwelling radiance measurements from the reference panel (gray or white panel depending on the current intensity of solar radiance) were collected to calibrate the upwelling radiance. The spectra were characterized with a range from 350 to 1050 nm and an interval of 1 nm. For details of the measurement and calculation of remote sensing reflectance above the water surface, the reader is referred to Shi, et al. [4].

Table 1. Sampling date, number, and parameters for four cruises in Lake Taihu and Hangzhou Bay during 2013, 2014, 2015, and 2017.

Sampling date	Number of samples	Sampling site	Parameters
5-10 August 2013	60	Lake Taihu	TSM, ISM, OSM, $a_p(\lambda)$, $a_{CDOM}(\lambda)$, $R_{rs}(\lambda)$
4-6 August 2014	60	Lake Taihu	TSM, ISM, OSM, $a_p(\lambda)$, $a_{CDOM}(\lambda)$, $R_{rs}(\lambda)$
16-18 April 2015	30	Lake Taihu	TSM, ISM, OSM, $a_p(\lambda)$, $a_{CDOM}(\lambda)$, $R_{rs}(\lambda)$
22-24 July 2017	50	Hangzhou Bay	TSM, ISM, OSM, $a_p(\lambda)$, $a_{CDOM}(\lambda)$, $R_{rs}(\lambda)$

2.3 Image acquisition and processing

The GOCI, a geostationary satellite ocean color sensor, was launched by South Korea in June 2010. GOCI satellite image data are characterized by high spatial resolution (500 m) and very high temporal resolution (1 h) and can obtain eight images for a certain location in a day. The GOCI has six visible bands and two NIR bands with center wavelengths of 412, 443, 490, 555, 660, 680, 745, and 865 nm. The zenith angle of GOCI is larger than that of the Moderate Resolution Imaging Spectroradiometer (MODIS) or Medium Resolution Imaging Spectrometer (MERIS), indicating that it has a longer optical path than these polar orbit satellites.

Optics EXPRESS

Level-1B data for Lake Taihu and Hangzhou Bay were freely download from the Korea Ocean Satellite Center (KOSC, https://kosc.kiost.ac.kr/). Chain operations such as region defining, cloud masking, Rayleigh correction, and atmospheric correction were all performed in SeaDAS 7.3. Level-1B data were atmospherically corrected with the Management Unit of North Sea Mathematical Models (MUMM) [33] algorithm. Traditional atmospheric correction based on the black pixel assumption in the NIR region will underestimate the water surface reflectance over turbid waters since the water-leaving radiances of turbid waters in NIR regions are not zero [34]. In the MUMM algorithm, this assumption is replaced by the assumption of spatial coincidence in the ratio of aerosol reflectance at 765 nm and 865 nm, as well as water surface reflectance. Compared with the standard algorithm over turbid inland or coastal water, the MUMM algorithm shows significant improvement and has been widely used for monitoring water parameters in turbid waters [35,36].

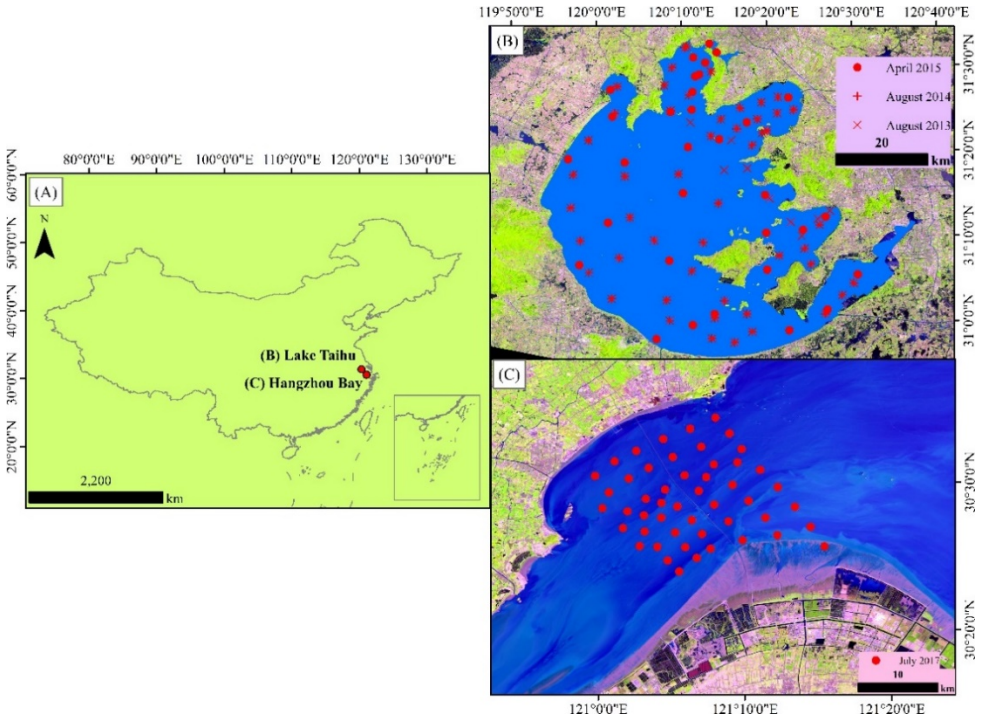

Fig. 1. Locations of Lake Taihu and Hangzhou Bay (A) and distribution of sampling sites in Lake Taihu (B) and Hangzhou Bay (C).

2.4 Model used for TSM estimation

In this study, we retrieve TSM by calculating the backscattering and absorption coefficients of suspended matter based on a semi-analytical method. The subsurface remote sensing reflectance ($r_{rs}(\lambda)$) was defined by Gordon, et al. [21]:

$$r_{rs}(\lambda) = \frac{f'}{Q}\frac{b_b(\lambda)}{a(\lambda)+b_b(\lambda)} \quad (1)$$

where $a(\lambda)$ is the total absorption coefficient, which includes the absorption of TSM, CDOM, and pure water; $b_b(\lambda)$ is the total backscattering coefficient, which includes the backscattering coefficients of TSM, CDOM, and pure water; f' is a dimensionless factor; and Q is ratio of upwelling irradiance to radiance of the water subsurface. The value of f'/Q is set to 0.13 according to Loisel and Morel [37]. $r_{rs}(\lambda)$ is related to the water-leaving reflectance ($\rho_w(\lambda)$):

Optics EXPRESS

$$\rho_w(\lambda) = \pi \Re r_{rs}(\lambda) \quad (2)$$

where $\Re$ = 0.53 is from Morel and Gentili [38] and combining Eqs. (1)-(2) gives the following:

$$b_b(\lambda) = a(\lambda)\frac{\rho_w(\lambda)}{f'\pi\Re/Q - \rho_w(\lambda)} \quad (3)$$

$\rho_w(\lambda)$ can also be related to the water surface remote sensing reflectance ($R_{rs}(\lambda)$) as follows:

$$\rho_w(\lambda) = \pi R_{rs}(\lambda) \quad (4)$$

Combining Eqs. (3)-(4) gives the following:

$$b_b(\lambda) = \frac{R_{rs}(\lambda)}{f'\Re/(Qa(\lambda)) - R_{rs}(\lambda)} \quad (5)$$

For ISM-dominated water, the backscattering coefficient of TSM ($b_{bp}(\lambda)$) is proportional to the TSM concentration through the specific backscatter coefficient of TSM, $b_{bp}^*(\lambda)$:

$$b_{bp}(\lambda) = \mathrm{TSM} \times b_{bp}^*(\lambda) \quad (6)$$

where $b_{bp}(\lambda)$ can be expressed as follows:

$$b_{bp}(\lambda) = b_b(\lambda) - b_{bw}(\lambda) \quad (7)$$

Therefore, the first indices, X_1, for the complex proxy can be expressed by the reflectance as follows:

$$X_1 \propto \frac{R_{rs}(\lambda)}{f'\Re/(Qa(\lambda)) - R_{rs}(\lambda)} \quad (8)$$

We use a three-band proxy of $R_{rs}(\lambda)$ to derive $a_p(\lambda)$ from $R_{rs}(\lambda)$:

$$a_p(\lambda_1) = [R_{rs}(\lambda_1)^{-1} - R_{rs}(\lambda_2)^{-1}] \times R_{rs}(\lambda_3) \times a_{water}(\lambda_3) + a_{water}(\lambda_2) - a_{water}(\lambda_1) \quad (9)$$

The three-band proxy of $R_{rs}(\lambda)$ in Eq. (9) can be made immune to the effects of CDOM absorption and particulate backscatter by choosing three appropriate wavelengths; therefore, $a_p(\lambda)$ is primarily determined by $R_{rs}(\lambda)$. To achieve this goal, λ_1, λ_2, and λ_3 should meet three requirements: (i) $a_{CDOM}(\lambda_1) \sim a_{CDOM}(\lambda_2)$; (ii) $a_p(\lambda_1) >> a_p(\lambda_2)$; and (iii) $a(\lambda_3) \sim a_{water}$.

Thus, the second indices, X_2, for the complex proxy can be expressed as follows:

$$X_2 \propto a_p(\lambda_1) = [R_{rs}(\lambda_1)^{-1} - R_{rs}(\lambda_2)^{-1}] \times R_{rs}(\lambda_3) \times a_{water}(\lambda_3) + a_{water}(\lambda_2) - a_{water}(\lambda_1) \quad (10)$$

Finally, a complex model (C_{TSM}) can be established from the above two indices as follows:

$$C_{TSM} = W_1 * X_1 + W_2 * X_2 \quad (11)$$

where W_1 and W_2 are weights that can be defined as the normalized determination coefficient between each index and the *in situ* TSM concentration.

2.5 Performance evaluation

Linear regressions and *t*-tests were performed using MATLAB R2012a. Results with $P<0.05$ in *t*-tests are reported as significant. The performance of proposed model in this research was evaluated based on the mean relative error (MRE), root mean square error (RMSE), and normalized root mean square error (NRMSE) as follows:

$$\mathrm{MRE} = 100\% \times \frac{1}{n}\sum_{i=1}^{n}\left|\frac{X_{esti,i} - X_{meas,i}}{X_{esti,i}}\right| \quad (12)$$

$$\mathrm{RMSE}=\sqrt{\frac{1}{\mathrm{n}}\sum_{i=1}^{n}(\mathrm{X}_{\mathrm{esti},i}-\mathrm{X}_{\mathrm{meas},i})^2} \tag{13}$$

$$\mathrm{NRMSE}=100\%\times\sqrt{\frac{1}{n}\sum_{i=1}^{n}(\mathrm{X}_{\mathrm{esti},i}-\mathrm{X}_{\mathrm{meas},i})^2}\Big/\left(\frac{1}{N}\sum_{i=1}^{N}\mathrm{X}_{\mathrm{meas},i}\right) \tag{14}$$

where X_{meas} and X_{esti} are the *in situ* measured and derived values and n is the number of data in the calculation.

3. Result

3.1 Water quality characterization

The sampling sites covered a wide range of TSM compositions and absorption coefficients (Table 2). In Lake Taihu, the TSM, ISM, OSM, $a_p(550)$, and $a_{CDOM}(254)$ values were 2.4-266.5 mg/L, 0.3-183.0 mg/L, 1.5-89.6 mg/L, 0.1-16.9 m^{-1}, and 0.3-38.2 m^{-1}, respectively. The maximum values of TSM, ISM, OSM, $a_p(550)$ and $a_{CDOM}(254)$ were 111-, 572-, 59-, 188-, and 119-fold larger than the minimum values, respectively.

In Hangzhou Bay, the TSM, ISM, OSM, $a_p(550)$ and $a_{CDOM}(254)$ values were 33.9-695.2 mg/L, 28.7-675.7 mg/L, 0.5-19.5 mg/L, 0.6-12.9 m^{-1}, and 8.2-11.8 m^{-1}. The maximum values of TSM, ISM, OSM, and $a_p(550)$ were 21-, 24-, 43- and 23-fold larger than the minimum values. However, $a_{CDOM}(254)$ exhibited a small range with low coefficients of variation.

TSM, ISM, OSM, $a_p(550)$ and $a_{CDOM}(254)$ in Hangzhou Bay exhibited smaller ranges with lower coefficients of variation compared with the values in Lake Taihu. The mean values of TSM, ISM, and $a_p(550)$ in Hangzhou Bay were 6-, 7-, and 2-fold higher than those in Lake Taihu. However, there was little difference in the mean OSM and $a_{CDOM}(254)$ between Hangzhou Bay and Lake Taihu.

Table 2. Statistics of the measured parameters (TSM; ISM; OSM; $a_p(550)$; $a_{CDOM}(254)$) for Lake Taihu and Hangzhou Bay. Coefficient of variation (CV) = SD/Mean.

Name	Parameter	Min	Max	Median	Mean	SD	CV
Lake Taihu (n = 153)	TSM, mg/L	2.4	266.5	28.9	21.9	31.9	1.5
	ISM, mg/L	0.3	183.0	15.7	17.7	25.5	1.4
	OSM, mg/L	1.5	89.6	10.4	7.7	12.9	1.7
	$a_p(550)$, m^{-1}	0.1	16.9	1.0	1.4	2.2	1.5
	$a_{CDOM}(254)$, m^{-1}	0.3	38.2	14.8	11.9	9.2	0.8
Hangzhou Bay (n = 50)	TSM, mg/L	33.9	695.2	93.0	127.7	130.3	1.0
	ISM, mg/L	28.7	675.7	84.2	122.2	127. 7	1.0
	OSM, mg/L	0.5	19.5	5.1	5.6	4.1	0.7
	$a_p(550)$, m^{-1}	0.6	12.9	2.6	2.9	2.4	0.8
	$a_{CDOM}(254)$, m^{-1}	8.2	11.8	9.3	9.4	0.7	0.1

3.2 Comparison of parameters and spectra

Figure 2(A), 2(B) show that the determination coefficient between TSM and ISM concentrations was 0.86 (P<0.001) for Lake Taihu and 0.999 (P<0.001) for Hangzhou Bay, whereas the determination coefficient between TSM and OSM was only 0.40 (P<0.001) for Lake Taihu and 0.41(P<0.001) for Hangzhou Bay. Therefore, TSM was dominated by ISM and not OSM in the turbid Lake Taihu and Hangzhou Bay.

In addition, more than 70% of samples in Lake Taihu had a value of ISM/OSM >1, but less than 30% samples had an OSM concentration higher than the ISM. By contrast, 100% of

Optics EXPRESS

samples from Hangzhou Bay had a value of ISM/OSM >1 (Fig. 2(C), 2(D)). These results indicate that TSM is primarily controlled by inorganic matter in Lake Taihu and Hangzhou Bay.

The absorption spectra of CDOM and TSM were also compared between Lake Taihu and Hangzhou Bay (Fig. 3). Generally, $a_p(\lambda)$ was significantly larger in Lake Taihu than in Hangzhou Bay in the visible and NIR regions. The $a_p(\lambda)$ spectra in Lake Taihu correspond approximately with the features of phytoplankton pigment, and an apparent maximum around 680 nm was observed in Lake Taihu due to the high absorption by phytoplankton pigments. There was no such feature in Hangzhou Bay, and $a_p(\lambda)$ exhibited typical exponential spectral shapes.

The $a_{CDOM}(\lambda)$ of the spectra was much lower than $a_p(\lambda)$ in both Taihu and Hangzhou Bay. The magnitude of the spectra of Taihu and Hangzhou Bay were very similar, and both exhibited typical exponential spectral shapes. In the green and red band (550-700 nm), $a_{CDOM}(\lambda)$ was extremely low in both Taihu and Hangzhou bay, with values close to 0.

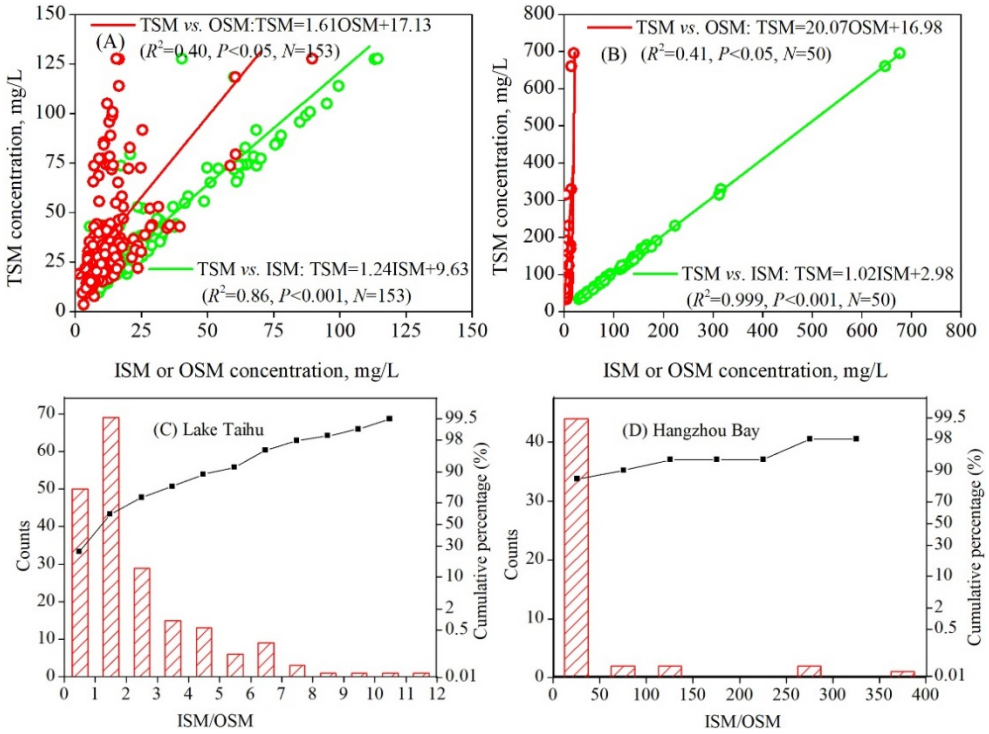

Fig. 2. Relationships between TSM and OSM or ISM for Lake Taihu (A) and Hangzhou Bay (B) and histogram distribution of ISM/OSM for Lake Taihu (C) and Hangzhou Bay (D).

Optics EXPRESS

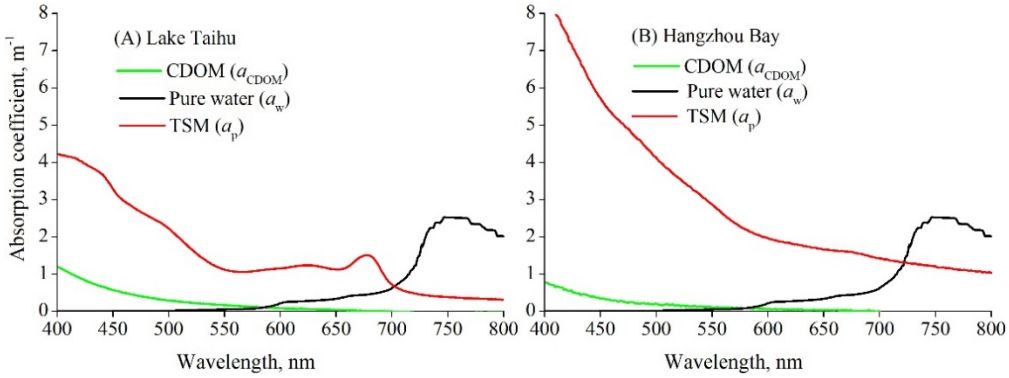

Fig. 3. Average absorption coefficients of CDOM, pure water, and TSM in Lake Taihu (A) and Hangzhou Bay (B).

3.3 Accuracy of atmospheric correction

By calculating the ratio of 765:865 nm for field observations of water-leaving reflectance, we found that the ratio for water reflectance over a water body was nearly spatially homogeneous, with values of 1.61 ± 0.11 in Hangzhou Bay, and 1.94 ± 0.14 in Lake Taihu, thus fulfilling the assumptions of the MUMM algorithm. The *in situ* reflectance measured by ASD measurements was simulated with GOCI spectral response functions to yield $R_{rs}(\lambda)$ values for the eight GOCI bands. The accuracy of the MUMM algorithm was evaluated by comparing the GOCI-derived and *in situ* simulated $R_{rs}(\lambda)$ for the highly turbid Lake Taihu and Hangzhou Bay (Fig. 4). Figure 4(C) and Fig. 4(F) show the NRMSE between the GOCI-derived and *in situ* simulated $R_{rs}(\lambda)$ values at eight GOCI bands, including the *in situ* $R_{rs}(\lambda)$ collected in Lake Taihu (August 7–9, 2013 (45 measurements)), and Hangzhou Bay (July 22–24, 2017 (47 measurements)). The GOCI-derived $R_{rs}(\lambda)$ is reasonable in the visible bands, except an underestimation of $R_{rs}(\lambda)$ at 660 nm in the extremely turbid Hangzhou Bay, which could be attributed to the decrease in water reflectance after saturation at short wavelengths [39]. For Hangzhou Bay and Lake Taihu, the NRMSE values at 412, 443, 490, 555, 660, 680, and 745 nm were less than 35%, and the largest error was found at 865 nm (NRMSE > 40%), whereas the lowest error was at 660 nm (NRMSE < 20%). Overall, the GOCI-derived and *in situ* measured $R_{rs}(\lambda)$ were evenly distributed along the 1:1 line.

Optics EXPRESS

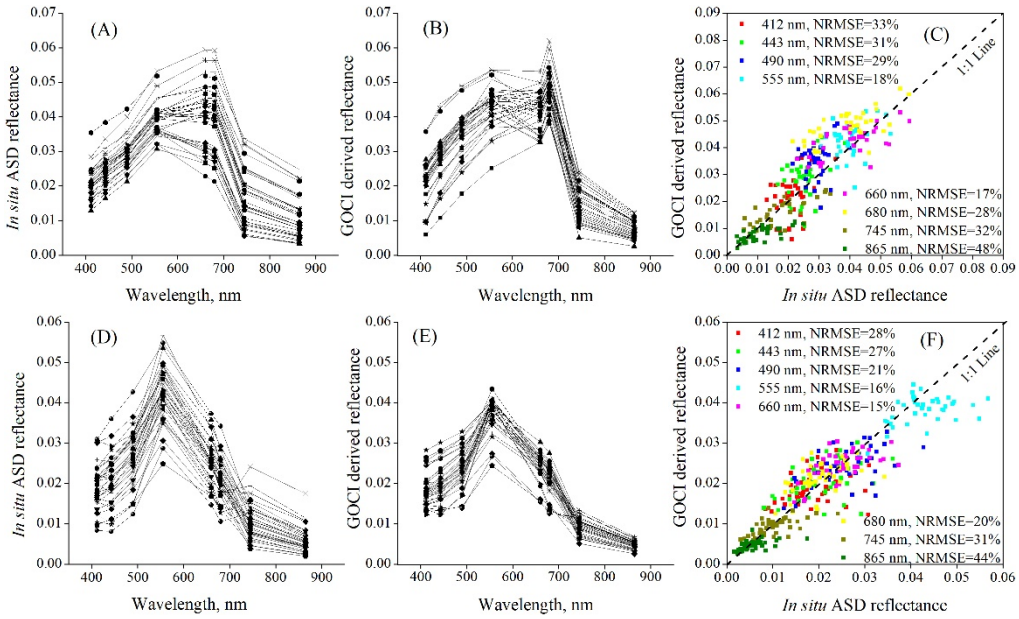

Fig. 4. Comparison between *in situ* measured and GOCI-derived $R_{rs}(\lambda)$. The *in situ* measured reflectance corresponded to the GOCI bands for Hangzhou Bay (A) and Lake Taihu (D). The spectra of the GOCI-derived $R_{rs}(\lambda)$ with the MUMM atmospheric correction method for Hangzhou Bay (B) and Lake Taihu (E). The linear regression between the *in situ* measured and GOCI-derived $R_{rs}(\lambda)$ for Hangzhou Bay (C) and Lake Taihu (F).

3.4 Model calibration

In Eq. (8), X_1 is still affected by $a_p(\lambda)$ in addition to $R_{rs}(\lambda)$. This could be avoided by choosing longer red or NIR wavelengths, where the total absorption is mainly from pure water. We assumed that backscattering by CDOM was negligible, and to determine the most appropriate position, we tuned the positions through iteration between TSM and *in situ* $R_{rs}(\lambda)$ in Eq. (8). Figure 5 indicates that the determination coefficient between the derived $b_{bp}(\lambda)$ and TSM concentration increased from the blue to red regions (400-700 nm) and reached the maximum in the NIR region.

For Hangzhou Bay and Lake Taihu, the TSM is highly related to the derived $b_{bp}(\lambda)$, with determination coefficients higher than 0.80 and NRMSE lower than 40% in the NIR region, especially in the 730-825 nm region (blue rectangular box in Fig. 5(A)). For the specific wavelength of 750 nm (corresponding to the GOCI center wavelength of band 7), the determination coefficient between the TSM concentration and derived $b_{bp}(\lambda)$ was 0.90 (Fig. 5(B)), and MRE, RMSE, and NRMSE were 18%, 19.3 mg/L and 28%. Separately, for the only Hangzhou Bay data set, R^2, MRE, RMSE and NRMSE were 0.89, 14%, 27.9 mg/L, and 22%; for the Lake Taihu data sets, R^2, MRE, RMSE and NRMSE were 0.81, 23%, 14.1 mg/L, and 33%.

Optics EXPRESS

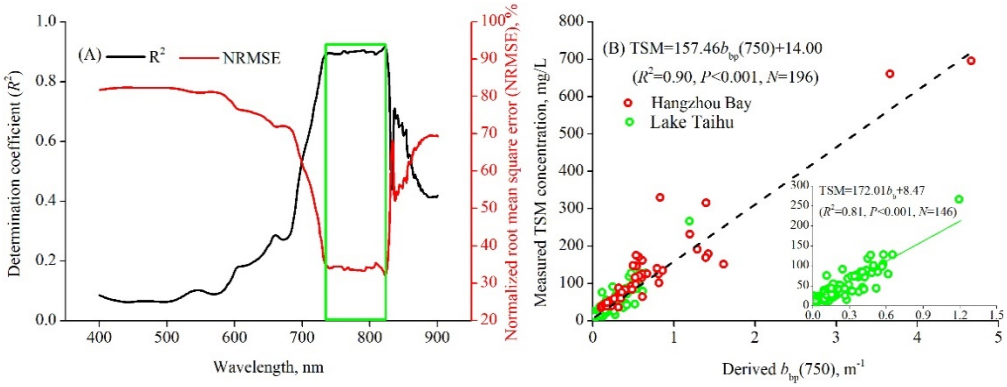

Fig. 5. R^2 and NRMSE between the TSM concentration and derived $b_{bp}(\lambda)$ based on Eq. (8) plotted as a function of wavelength for Hangzhou Bay and Lake Taihu (A). The relationship between the *in situ* TSM concentration and derived $b_{bp}(750)$ nm in Hangzhou Bay and Lake Taihu (B).

There are many candidate bands of λ_1, λ_2, and λ_3 for deriving $a_p(\lambda)$ in Eq. (9), and the three wavelengths may vary with water type. To find the most appropriate wavelengths of λ_1, λ_2, and λ_3 for Hangzhou Bay and Lake Taihu, we tuned the wavelengths of λ_1, λ_2, and λ_3 in Eq. (9) through three iterations between TSM and a proxy of three *in situ* $R_{rs}(\lambda_i)$ values (i = 1, 2 and 3). To seek the position of λ_3, we set the initial λ_1 = 540 nm and λ_2 = 700 nm, where $a_p(\lambda_1)>>a_p(\lambda_2)$ and $a_{CDOM}(\lambda_1)$ is quite close to $a_{CDOM}(\lambda_2)$. The proxy ($[R_{rs}^{-1}(540)-R_{rs}^{-1}(700)] \times R_{rs}(\lambda_3)$) was then regressed against the TSM concentration between 600 and 800 nm. The R^2 between the measured TSM concentration and the proxy gave high values when λ_3 was between 740 and 760 nm (Fig. 6(A)). In the second iteration, to seek the appropriate wavelengths for λ_1, we regressed $[R_{rs}^{-1}(\lambda_1) - R_{rs}^{-1}(700)] \times R_{rs}(750)$ against TSM. The R^2 was at a maximum when λ_1 was between 530 and 580 nm (Fig. 6(B)). In the third iteration, we found λ_2 by regressing $[R_{rs}^{-1}(550)-R_{rs}^{-1}(\lambda_2)] \times R_{rs}(750)$ vs. TSM. R^2 was a maximum for λ_2 over a range of 730–820 nm (Fig. 6(C)). Hence, λ_1, λ_2 and λ_3 were 550 nm, 750 nm and 750 nm, respectively, and the indices of X_2 could be exactly described as $a_{water}(750) \times [R_{rs}^{-1}(550)-R_{rs}^{-1}(750)] \times R_{rs}(750) + a_{water}(750)-a_{water}(550)$. The R^2 between the TSM concentration and derived $a_p(550)$ was 0.91 (Fig. 6(D)), and the MRE, RMSE, and NRMSE were 27%, 28.0 mg/L and 46%, respectively. Separately, for the only data set from Hangzhou Bay, R^2, MRE, RMSE and NRMSE were 0.92, 16%, 42.7 mg/L, and 34%; for the Lake Taihu data sets, R^2, MRE, RMSE and NRMSE were 0.71, 30%, 16.2 mg/L, and 37%. The results above indicate that the derivation of TSM was also sensitive to the second index X_2. Indeed, the three bands formed at 550 nm, 750 nm, and 750 nm could be rewritten as the band ratio of $R_{rs}(750)$ to $R_{rs}(550)$.

Optics EXPRESS

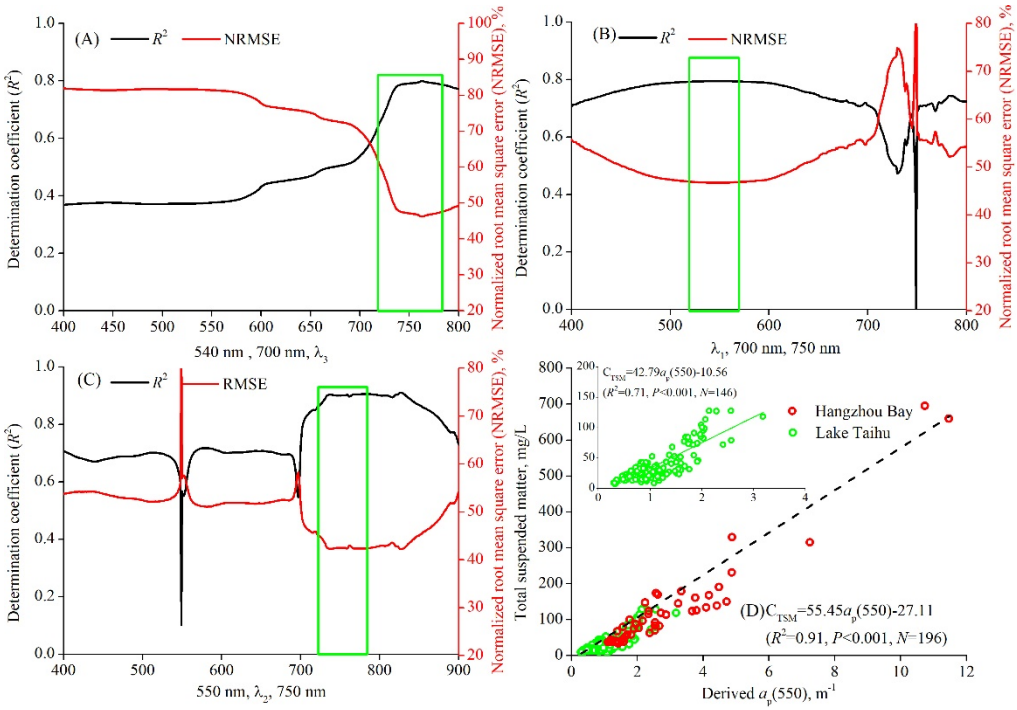

Fig. 6. R^2 and NRMSE in Hangzhou Bay and Lake Taihu between *in situ* TSM and the semi-analytical results plotted as a function of the wavelength in the first iteration (A), second iteration (B), and third iteration (C). The maximal values of R^2 and the minimum NRMSE were at 550 nm for λ_1, 750 nm for λ_2, and 750 nm for λ_3. (D) The relationship between *in situ* measured TSM and the derived $a_p(550)$ in Hangzhou Bay and Lake Taihu.

Finally, the C_{TSM} model (Eq. (11)) including X_1 and X_2 was constructed for deriving TSM in Hangzhou Bay and Lake Taihu, and W_1 and W_2 were defined as 0.48 and 0.52 for Hangzhou Bay and 0.76 and 0.24 for Lake Taihu.

3.5 Evaluation of model accuracy

To evaluate the C_{TSM} model and demonstrate its ability to retrieve TSM in Hangzhou Bay and Lake Taihu, two different data sets were used in this study—an *in situ* reflectance data set and atmospheric corrected GOCI data.

A match-up data set was constructed from the *in situ* measured TSM values and derived TSM concentrations. There are 50 stations in Hangzhou Bay and 146 stations in Lake Taihu.

The comparison between the TSM derived using ASD reflectance and the *in situ* TSM in Fig. 7(A) shows that most pairs are evenly distributed along a 1:1 line over a wide range of TSM. For the whole data sets of Hangzhou Bay and Lake Taihu, R^2, MRE, RMSE, and NRMSE are 0.94, 32%, 20.1 mg/L, and 33%, respectively, indicating that our proposed model with *in situ* ASD reflectance can explain 94% of the variance. Separately, for the Hangzhou Bay data set (n = 50), R^2, MRE, RMSE and NRMSE are 0.95, 17% 32.3 mg/L, and 25%, respectively; for the Lake Taihu data set (n = 146), R^2, MRE, RMSE and NRMSE are 0.85, 36%, 13.5 mg/L, and 34%, respectively. The derived TSM concentrations range from 33.9 to 695.3 mg/L in Hangzhou Bay and from 9.2 to 273.3 mg/L in Lake Taihu. The model exploited the different relationships between TSM concentration and multiband reflectance, which improved the performance and expanded the range for deriving TSM.

The GOCI-derived $R_{rs}(\lambda)$ values were also used to validate the model, and the time interval between the *in situ* measurement and GOCI overpass was <1 h. Figure 7(B) shows the validation results of the proposed model with GOCI data for Hangzhou Bay and Lake

Optics EXPRESS

Taihu. The *in situ* measured and GOCI-derived TSM values were distributed around the 1:1 line, and the determination coefficient was 0.83, indicating that our proposed model with GOCI-derived reflectance can explain 83% of the variance. In addition, MRE, RMSE, and NRMSE of TSM were 41%, 43.1 mg/L, and 55%. Separately, for the only data set of Hangzhou Bay (n = 50), R^2, MRE, RMSE and NRMSE were 0.78, 51%, 56.9 mg/L, and 44%; for the Lake Taihu data set (n = 62), R^2, and MRE, RMSE and NRMSE were 0.75, 45%, 12.9 mg/L, and 36%. The results above indicate that the C_{TSM} model proposed in this research can be used for TSM estimation in Hangzhou Bay and Lake Taihu with satisfactory accuracy and can thus facilitate studies of the dynamics of TSM and other related parameters in turbid waters.

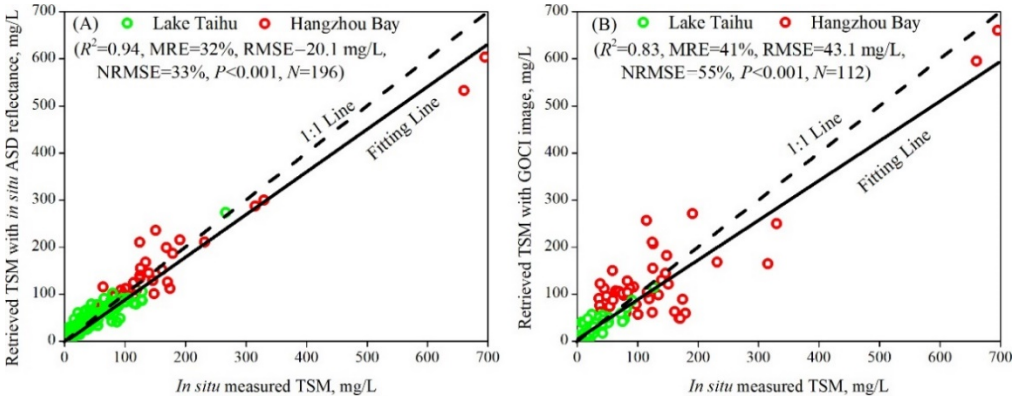

Fig. 7. Linear relationship between *in situ* measured and TSM concentrations derived from ASD reflectance (A) and GOCI-derived reflectance (B) for Hangzhou Bay and Lake Taihu.

4. Discussion

4.1 Model application and comparison

Inorganic particles dominated the absorption and backscattering processes in Hangzhou Bay and Lake Taihu [40], and the average $a_p(\lambda)$ was much larger than the $a_{CDOM}(\lambda)$ (Figs. 3(A) and 3(B)). Therefore, the effect of $a_{CDOM}(\lambda)$ could be negligible in deriving $a_p(\lambda)$ from $R_{rs}(\lambda)$. However, it is unknown if this C_{TSM} model is still valid in other water types. The Xin'anjiang Reservoir (China) is a deep valley reservoir with a low TSM concentration but a noticeably significant contribution of $a_{CDOM}(\lambda)$ to the total absorption [18]. To determine if the C_{TSM} model is still valid in the Xin'anjiang Reservoir, we derived $a_p(\lambda)$ and $b_{bp}(\lambda)$ in Eqs. (8)-(9) from the *in situ* reflectance. Figure 8 indicated that the derived $b_{bp}(750)$ did not show a significant relationship with the *in situ* TSM concentration (R^2 = 0.061, P<0.05) due to the small variations and low TSM concentration in the Xin'anjiang Reservoir [18]. Three iterations were also performed to identify the most appropriate positions of λ_1, λ_2, and λ_3 for deriving $a_p(\lambda)$ of the Xin'anjiang Reservoir (Fig. 9). The high R^2 (0.72) and low NRMSE (23%) between TSM and the derived $a_p(542)$ and the distribution of its relative error along with $a_{CDOM}(254)$ in Fig. 9(D) indicate that the form $R_{rs}^{-1}(\lambda_1) - R_{rs}^{-1}(\lambda_2)$ in Eq. (9) with appropriate λ_1 and λ_2 can minimize the effect of CDOM absorption in deriving $a_p(\lambda)$ and thus be used for TSM estimation in the slightly turbid Xin'anjiang Reservoir. In the past, it has been challenging to make clear the spectral dependency of optical components (TSM, chlorophyll *a*, and CDOM) due to the difficulty of measuring the absorption and backscattering coefficients of these components in highly turbid coastal, inland waters [41]. In addition, the lack of methods for isolating the absorption and backscattering coefficients of these components from remote sensing data has prevented an understanding of critical optical processes and properties. Therefore, the ability to derive the $a_p(\lambda)$ and $b_{bp}(\lambda)$ from remote sensing reflectance is of great interest for inland or coastal waters. However, it should be

Optics EXPRESS

emphasized that the proposed model is better used for ISM-dominated turbid water. For other waters with different bio-optical properties, the weight values of the two indices in the model may need to be modified on a case-by-case basis.

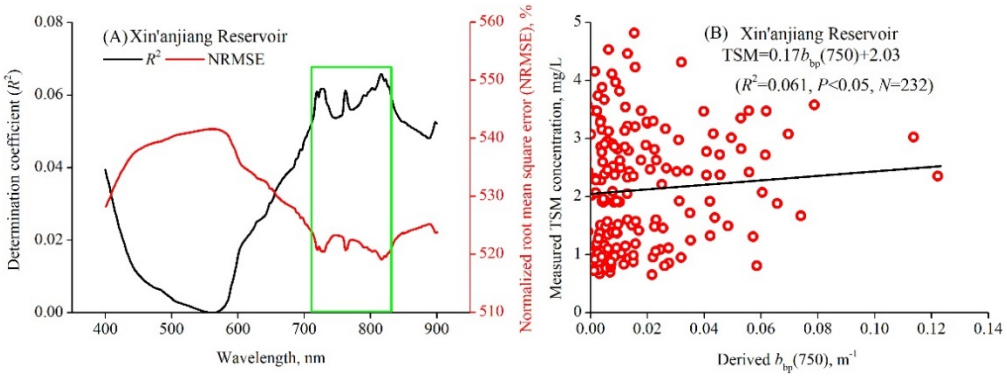

Fig. 8. R^2 and NRMSE between TSM concentration and derived $b_{bp}(\lambda)$ in the Xin'anjiang Reservoir based on Eq. (8) plotted as a function of wavelength (A); relationship between TSM concentration and derived $b_{bp}(750)$ in the Xin'anjiang Reservoir (B).

In this study, we did not measure $b_{bp}(\lambda)$. Figure 10 compares the derived $b_{bp}(\lambda)$ from our proposed model and the improved QAA algorithm (QAA_Le) [42]. The QAA_Le algorithm was developed for deriving $a_p(\lambda)$ and $b_{bp}(\lambda)$ for turbid water by altering the reference wavelength (λ_0) in the QAA algorithm [26] from 555 nm to 710 nm, where the total absorption is still dominated by pure water. The result indicated that the QAA_Le derived $b_{bp}(750)$ corresponded well with the $b_{bp}(750)$ derived by our model in Hangzhou Bay (MRE = 10%, RMSE = 0.1 m^{-1}, and NRMSE = 13%) and Lake Taihu (MRE = 45%, RMSE = 0.2 m^{-1}, and NRMSE = 47%) (Fig. 10). Both the QAA_Le algorithm and our proposed model showed satisfactory accuracy in deriving $a_p(550)$ in Hangzhou Bay (Fig. 11(A)). However, the QAA_Le-derived $a_p(550)$ did not agree with the *in situ* $a_p(550)$ in Lake Taihu (MRE = 98%, RMSE = 1.2 m^{-1}, and NRMSE = 107%). By contrast, the $a_p(550)$ derived from our model corresponded well with the *in situ* $a_p(550)$ in Lake Taihu (MRE = 22%, RMSE = 0.3 m^{-1}, and NRMSE = 28%) (Fig. 11(B)). The proposed model in this study was effective in deriving the $b_{bp}(750)$ and $a_p(550)$ from Lake Taihu and Hangzhou Bay, whereas the QAA_Le algorithm failed for these water bodies. This failure can be attributed to the fact that the reference wavelength in the QAA_Le algorithm varies and is empirically determined by the optical properties of water components. In addition, the power-law shape of the $a_p(\lambda)$ spectra in the QAA_Le algorithm omits any signal from phytoplankton.

A large of empirical models have been studied previously to estimate TSM in Lake Taihu and Hangzhou Bay [2,29,43–49]. The sensitivity indexes in these studies were used to model the relationship between $R_{rs}(\lambda)$ and TSM, and the performance of these adjusted models is also compared in Table 3. The model by He, et al. [29] worked well in Hangzhou Bay with high accuracy, while the accuracy greatly decreased for Lake Taihu (Fig. 12). The reflectance in NIR ($R_{rs}(745)$) is suggested for estimating high TSM [3,4,29,43], and therefore the ratio of $R_{rs}(745)$ to $R_{rs}(490)$ is significantly correlated with TSM in the highly turbid Hangzhou Bay, whereas this ratio did not match the *in situ* TSM in moderately or slightly turbid water. Instead, the sensitive wavelength should move to shorter wavelengths in moderately or slightly turbid water. For instance, in moderately turbid lakes/reservoirs and coastal water, the reflectance at 645 nm is usually used to estimate TSM with satisfactory accuracy [3,4,43]. However, a mismatch again appears when the derived TSM based on $R_{rs}(745)$ or $R_{rs}(645)$ is compared with the *in situ* TSM concentration in slightly turbid inland or open ocean water [6,10]. This mismatch can be partly attributed to the decreased ratio of signal to noise and confusion about the of optical properties of lower TSM. This mismatch can hopefully be

Optics EXPRESS

reduced if a semi-analytical algorithm is used. Although the semi-analytical algorithm may not necessarily demonstrate superior accuracy than empirical algorithms for a specific site or region, the semi-analytical approach can theoretically explain the relationship among the absorption, backscattering and reflectance of water optical components and could provide a general model for deriving TSM from chlorophyll *a* and CDOM estimates in different types of water.

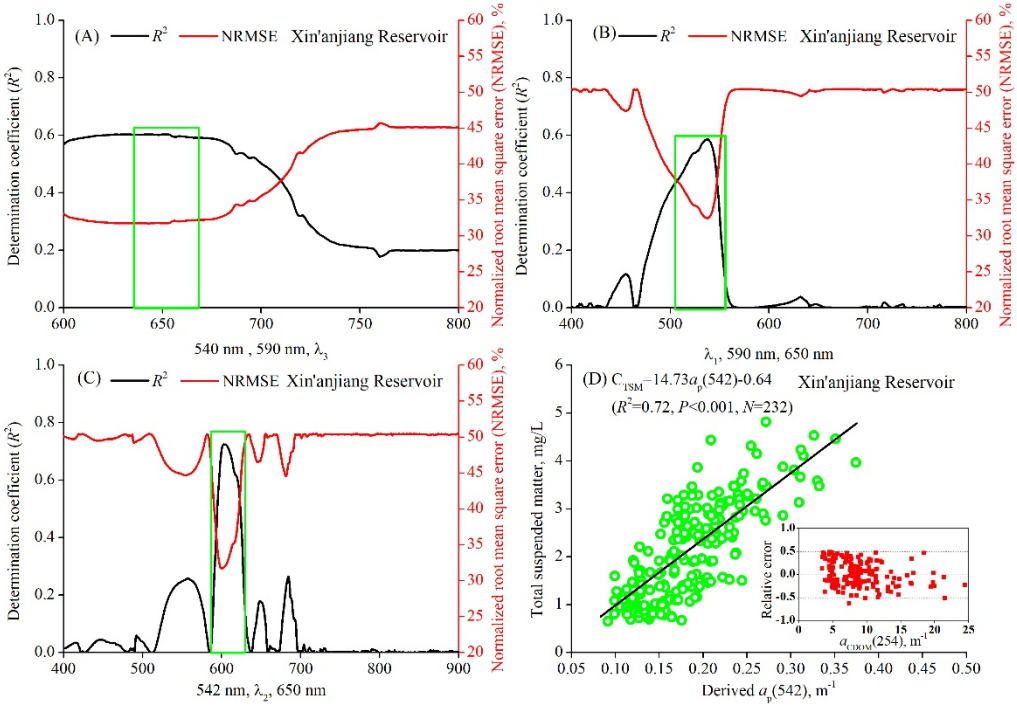

Fig. 9. R^2 and NRMSE between measured TSM concentration and semi-analytical model plotted as a function of wavelength for (A) λ_3, (B) λ_1, and (C) λ_2. The maximal values of R^2 and minimum NRMSE were at 542 nm for λ_1, at 600 nm for λ_2, and at 650 nm for λ_3. The relationship between the *in situ* TSM and derived $a_p(542)$ and the distribution of the relative error along with $a_{CDOM}(254)$ in the Xin'anjiang Reservoir (D).

The GOCI image has a high signal-to-noise ratio and offers hourly daylight observation [50]. The "self-sufficient" atmospheric correction for GOCI data with band 7 and band 8 performed well in highly turbid waters [51]. GOCI-II will be launched in the near future as a continuation of the present GOCI satellite. GOCI-II is thus expected to provide more images for water environment monitoring in inland waters, river estuaries and coastal regions. The proposed model in this research simplifies the traditional semi-analytical model and relies on only two GOCI bands (750 nm and 550 nm) as input for deriving $a_p(\lambda)$ and $b_{bp}(\lambda)$ and, consequently, TSM estimation. This work will facilitate the application of the GOCI satellite in observing sediment dynamics, plume evolution and erosion/sedimentation patterns based on hydrological activities, weather phenomena, and tidal forces in northeast Asia.

Optics EXPRESS

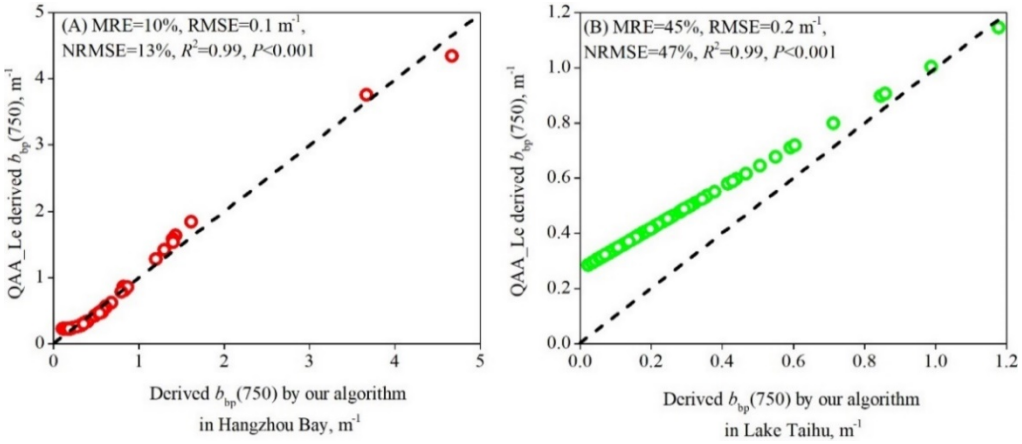

Fig. 10. Comparison of the $b_{bp}(750)$ values derived by QAA_Le and our model from remote sensing reflectance data in Hangzhou Bay and Lake Taihu.

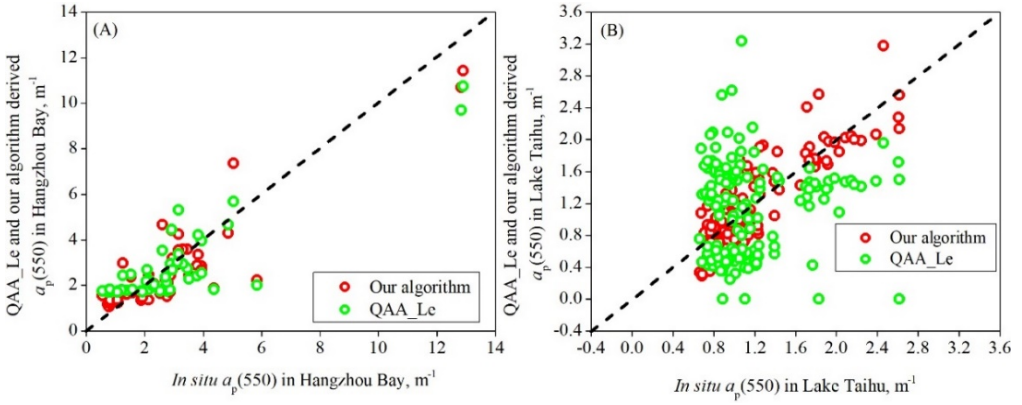

Fig. 11. Comparison of the $a_p(550)$ values derived by QAA_Le and our model from remote sensing reflectance data in Hangzhou bay and Lake Taihu.

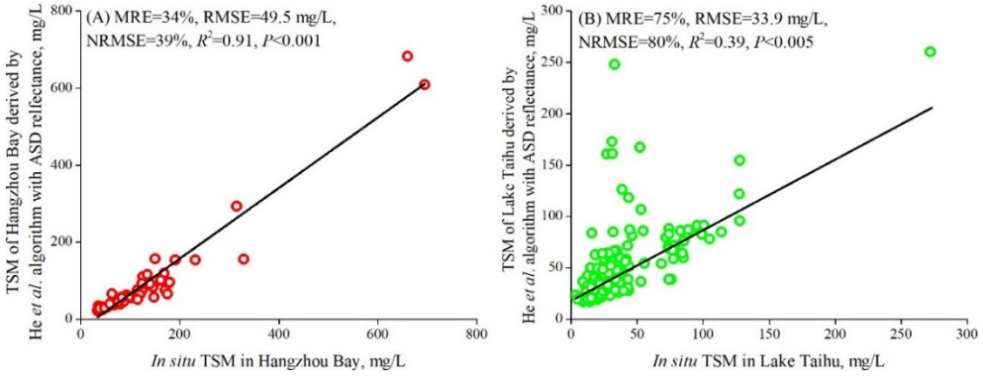

Fig. 12. Linear regression between TSM measured *in situ* and derived from ASD reflectance using the algorithm by He, et al. [29] for Hangzhou Bay (A) and Lake Taihu (B).

Table 3. Performance comparison of TSM estimation models for Lake Taihu and Hangzhou Bay.

Study area	Authors	Adjusted mode	R^2	NRMSE
Lake Taihu	Hou et al.[43]	TSM = 77.68$R_{rs}(645)/R_{rs}(555)$-14.24	0.21	131%

Optics EXPRESS

Lake Taihu	Huang et al. [44]	TSM = 123.16R_{rs}(745)/R_{rs}(555) + 2.73	0.72	64%
Lake Taihu	Zhang et al. [45]	TSM = 480.93R_{rs}(485) + 25.44	0.11	215%
Lake Taihu	Zhou et al. [46]	TSM = 1463R_{rs}(660) + 1.02	0.25	124%
Lake Taihu	Zhang et al. [2]	TSM = 2016.11R_{rs}(709)-13.82	0.64	75%
Hangzhou Bay	Mao et al. [47]	TSM = 98.08R_{rs}(670)/(0.085- R_{rs}(670)) + 3.12	0.48	93%
Hangzhou Bay	Mao et al. [47]	TSM = 176.9R_{rs}(765)/R_{rs}(443)-24.91	0.74	62%
Hangzhou Bay	Mao et al. [47]	TSM = 6478(R_{rs}(765) + R_{rs}(510))-196.98	0.61	85%
Hangzhou Bay	Zhang et al. [48]; Siswanto et al. [49]	Log_{10}TSM = 3.89 + 21.12(R_{rs}(555) + R_{rs}(645))-5.0(R_{rs}(488)/R_{rs}(555))	0.60	87%
Hangzhou Bay	He et al. [29]	Log_{10}TSM = 1.34 + 1.10* R_{rs}(745)/R_{rs}(490)	0.92	25%

5. Conclusions

In this study, a two-step, IOP-based model based on partitioning $a_p(550)$ and $b_{bp}(750)$ from remote sensing reflectance was developed for Lake Taihu and Hangzhou Bay. Our derived $b_{bp}(750)$ values agree well with those derived by QAA_Le for Hangzhou Bay (MRE = 10%, RMSE = 0.1 m^{-1}, and NRMSE = 13%) and Lake Taihu (MRE = 45%, RMSE = 0.2 m^{-1}, and NRMSE = 47%). Our approach is effective in predicting $a_p(550)$ in Lake Taihu, and the form $R_{rs}^{-1}(\lambda_1) - R_{rs}^{-1}(\lambda_2)$ minimizes the effect of CDOM absorption in deriving $a_p(\lambda)$. The $a_p(550)$ and $b_{bp}(750)$ are weighted according to the determination coefficient between each index and the TSM concentration and thus can be used to derive TSM. The derived TSM based on the *in situ* reflectance and GOCI images both correspond well with the *in situ* measured TSM with low MRE (32%, 41%), RMSE (20.1 mg/L, 43.1 mg/L), and NRMSE (33%, 55%). The model exploits the different relationships between TSM concentration and multiband reflectance, thus improving the performance and broadening the range for deriving TSM.

Funding

Key Research Program of Frontier Sciences, Chinese Academy of Sciences (QYZDB-SSW-DQC016); National Natural Science Foundation of China (41621002, 41771472 and 41501374), Youth Innovation Promotion Association (CAS) (2017365); Zhejiang Provincial Natural Science Foundation of China (LQ16D010001).

Acknowledgments

We would like to thank Yubing Deng, Yaoduo Hu, Zhong Xia, Yang Bai, Huiming Zha for their participation in the field samples collection. We appreciate Korea Ocean Satellite Center for providing GOCI images. We also include an acknowledgment to thank the two anonymous reviewers for their useful reviews for this paper.

Disclosures

The authors declare no conflicts of interest.

References

1. Z. Mao, D. Pan, C. L. Tang, B. Tao, J. Chen, Y. Bai, P. Chen, X. He, Z. Hao, H. Huang, and Q. Zhu, "A dynamic sediment model based on satellite-measured concentration of the surface suspended matter in the East China Sea," J. Geophys. Res. **121**(4), 2755–2768 (2016).
2. Y. Zhang, K. Shi, X. Liu, Y. Zhou, and B. Qin, "Lake topography and wind waves determining seasonal-spatial dynamics of total suspended matter in turbid Lake Taihu, China: assessment using long-term high-resolution MERIS data," PLoS One **9**(5), e98055 (2014).

Optics EXPRESS

3. Y. Zhang, K. Shi, Y. Zhou, X. Liu, and B. Qin, "Monitoring the river plume induced by heavy rainfall events in large, shallow, Lake Taihu using MODIS 250 m imagery," Remote Sens. Environ. **173**, 109–121 (2016).
4. K. Shi, Y. Zhang, G. Zhu, X. Liu, Y. Zhou, H. Xu, B. Qin, G. Liu, and Y. Li, "Long-term remote monitoring of total suspended matter concentration in Lake Taihu using 250m MODIS-Aqua data," Remote Sens. Environ. **164**, 43–56 (2015).
5. A. A. Corcoran, K. M. Reifel, B. H. Jones, and R. F. Shipe, "Spatiotemporal development of physical, chemical, and biological characteristics of stormwater plumes in Santa Monica Bay, California (USA)," J. Sea Res. **63**(2), 129–142 (2010).
6. M. Ondrusek, E. Stengel, C. S. Kinkade, R. L. Vogel, P. Keegstra, C. Hunter, and C. Kim, "The development of a new optical total suspended matter algorithm for the Chesapeake Bay," Remote Sens. Environ. **119**, 243–254 (2012).
7. C. Giardino, V. E. Brando, A. G. Dekker, N. Strömbeck, and G. Candiani, "Assessment of water quality in Lake Garda (Italy) using Hyperion," Remote Sens. Environ. **109**(2), 183–195 (2007).
8. M. J. Moreno-Madriñán and A. M. Fischer, "Performance of the MODIS FLH algorithm in estuarine waters: a multi-year (2003–2010) analysis from Tampa Bay, Florida (USA)," Int. J. Remote Sens. **34**(19), 6467–6483 (2013).
9. V. Volpe, S. Silvestri, and M. Marani, "Remote sensing retrieval of suspended sediment concentration in shallow waters," Remote Sens. Environ. **115**(1), 44–54 (2011).
10. A. G. Dekker, R. J. Vos, and S. W. M. Peters, "Comparison of remote sensing data, model results and in situ data for total suspended matter (TSM) in the southern Frisian lakes," Sci. Total Environ. **268**(1-3), 197–214 (2001).
11. M. Lei, A. Minghelli, M. Fraysse, I. Pairaud, R. Verney, and C. Pinazo, "Geostationary image simulation on coastal waters using hydrodynamic biogeochemical and sedimentary coupled models," IEEE J. Sel. Top. Appl. Earth Obs. Remote Sens. **9**(11), 5209–5222 (2016).
12. C. Mitchell and A. Cunningham, "Remote sensing of spatio-temporal relationships between the partitioned absorption coefficients of phytoplankton cells and mineral particles and euphotic zone depths in a partially mixed shelf sea," Remote Sens. Environ. **160**, 193–205 (2015).
13. C. B. Mouw, H. Chen, G. A. Mckinley, S. Effler, D. O'Donnell, M. G. Perkins, and C. Strait, "Evaluation and optimization of bio-optical inversion algorithms for remote sensing of Lake Superior's optical properties," J. Geophys. Res. **118**(4), 1696–1714 (2013).
14. D. Odermatt, A. Gitelson, V. E. Brando, and M. Schaepman, "Review of constituent retrieval in optically deep and complex waters from satellite imagery," Remote Sens. Environ. **118**, 116–126 (2012).
15. L. Feng, C. Hu, X. Chen, and Q. Song, "Influence of the Three Gorges Dam on total suspended matters in the Yangtze Estuary and its adjacent coastal waters: Observations from MODIS," Remote Sens. Environ. **140**, 779–788 (2014).
16. R. P. Stumpf, R. A. Arnone, R. W. Gould, P. M. Martinolich, and V. Ransibrahmanakul, "A partially coupled ocean-atmosphere model for retrieval of water-leaving radiance from SeaWiFS in coastal waters, SeaWiFS postlaunch," Tech. Rep. Ser. (World Health Organ.) **22**, 51–59 (2003).
17. D. Doxaran, J. M. Froidefond, S. Lavender, and P. Castaing, "Spectral signature of highly turbid waters," Remote Sens. Environ. **81**(1), 149–161 (2002).
18. Y. Zhang, Y. Zhang, K. Shi, Y. Zha, Y. Zhou, and M. Liu, "A Landsat 8 OLI-based, semianalytical model for estimating the total suspended matter concentration in the slightly turbid Xin'anjiang Reservoir (China)," IEEE J. Sel. Top. Appl. Earth Obs. Remote Sens. **9**(1), 398–413 (2016).
19. G. Zheng and P. M. Digiacomo, "Uncertainties and applications of satellite-derived coastal water quality products," Prog. Oceanogr. **159**, 45–72 (2017).
20. S. Koponen, J. Attila, J. Pulliainen, K. Kallio, T. Pyhalahti, A. Lindfors, K. Rasmus, and M. Hallikainen, "A case study of airborne and satellite remote sensing of a spring bloom event in the Gulf of Finland," Cont. Shelf Res. **27**(2), 228–244 (2007).
21. H. R. Gordon, O. B. Brown, R. H. Evans, J. W. Brown, R. C. Smith, K. S. Baker, and D. K. Clark, "A semianalytic radiance model of ocean color," J. Geophys. Res. **93**(D9), 10909–10924 (1988).
22. M. Babin, A. Morel, V. Fournier-Sicre, F. Fell, and D. Stramski, "Light scattering properties of marine particles in coastal and open ocean waters as related to the particle mass concentration," Limnol. Oceanogr. **48**(2), 843–859 (2003).
23. S. B. Woźniak, D. Stramski, M. Stramska, R. A. Reynolds, V. M. Wright, E. Y. Miksic, M. Cichocka, and A. M. Cieplak, "Optical variability of seawater in relation to particle concentration, composition, and size distribution in the nearshore marine environment at Imperial Beach, California," J. Geophys. Res. **115**(C8), C08027 (2010).
24. C. E. Binding, J. H. Jerome, R. P. Bukata, and W. G. Booty, "Suspended particulate matter in Lake Erie derived from MODIS aquatic colour imagery," Int. J. Remote Sens. **31**(19), 5239–5255 (2010).
25. M. Babin and D. Stramski, "Light absorption by aquatic particles in the near□infrared spectral region," Limnol. Oceanogr. **47**(3), 911–915 (2002).
26. Z. Lee, K. L. Carder, and R. A. Arnone, "Deriving inherent optical properties from water color: a multiband quasi-analytical algorithm for optically deep waters," Appl. Opt. **41**(27), 5755–5772 (2002).
27. B. Qin, P. Xu, Q. Wu, L. Luo, and Y. Zhang, "Environmental issues of Lake Taihu, China," Hydrobiologia **581**(1), 3–14 (2007).

Optics EXPRESS

28. D. Xie, Z. Wang, S. Gao, and H. J. De Vriend, "Modeling the tidal channel morphodynamics in a macro-tidal embayment, Hangzhou Bay, China," Cont. Shelf Res. **29**(15), 1757–1767 (2009).
29. X. He, Y. Bai, D. Pan, N. Huang, X. Dong, J. Chen, C.-T. A. Chen, and Q. Cui, "Using geostationary satellite ocean color data to map the diurnal dynamics of suspended particulate matter in coastal waters," Remote Sens. Environ. **133**, 225–239 (2013).
30. Y. Zhang, B. Zhang, X. Wang, J. Li, S. Feng, Q. Zhao, M. Liu, and B. Qin, "A study of absorption characteristics of chromophoric dissolved organic matter and particles in Lake Taihu, China," Hydrobiologia **592**(1), 105–120 (2007).
31. Y. Zhang, Y. Zhou, K. Shi, B. Qin, X. Yao, and Y. Zhang, "Optical properties and composition changes in chromophoric dissolved organic matter along trophic gradients: Implications for monitoring and assessing lake eutrophication," Water Res. **131**, 255–263 (2018).
32. C. D. Clark, L. P. Litz, and S. B. Grant, "Saltmarshes as a source of chromophoric dissolved organic matter (CDOM) to Southern California coastal waters," Limnol. Oceanogr. **53**(5), 1923–1933 (2008).
33. K. G. Ruddick, F. Ovidio, and M. Rijkeboer, "Atmospheric correction of SeaWiFS imagery for turbid coastal and inland waters," Appl. Opt. **39**(6), 897–912 (2000).
34. C. Hu, K. L. Carder, and F. E. Muller-Karger, "Atmospheric correction of SeaWiFS imagery over turbid coastal waters: A practical method," Remote Sens. Environ. **74**(2), 195–206 (2000).
35. J. K. Choi, Y. J. Park, J. H. Ahn, H. S. Lim, J. Eom, and J. H. Ryu, "GOCI, the world's first geostationary ocean color observation satellite, for the monitoring of temporal variability in coastal water turbidity," J. Geophys. Res. **117**(C9), 9004 (2012).
36. B. Nechad, K. G. Ruddick, and Y. Park, "Calibration and validation of a generic multisensor algorithm for mapping of total suspended matter in turbid waters," Remote Sens. Environ. **114**(4), 854–866 (2010).
37. H. Loisel and A. Morel, "Non-isotropy of the upward radiance field in typical coastal (Case 2) waters," Int. J. Remote Sens. **22**(2-3), 275–295 (2001).
38. A. Morel and B. Gentili, "Diffuse reflectance of oceanic waters. III. Implication of bidirectionality for the remote-sensing problem," Appl. Opt. **35**(24), 4850–4862 (1996).
39. M. Wang, W. Shi, and L. Jiang, "Atmospheric correction using near-infrared bands for satellite ocean color data processing in the turbid western Pacific region," Opt. Express **20**(2), 741–753 (2012).
40. D. Sun, Y. Li, Q. Wang, H. Lv, C. Le, C. Huang, and S. Gong, "Partitioning particulate scattering and absorption into contributions of phytoplankton and non-algal particles in winter in Lake Taihu (China)," Hydrobiologia **644**(1), 337–349 (2010).
41. W. Zhou, G. Wang, Z. Sun, W. Cao, Z. Xu, S. Hu, and J. Zhao, "Variations in the optical scattering properties of phytoplankton cultures," Opt. Express **20**(10), 11189–11206 (2012).
42. Y. Zha, D. Sun, and B. Yin; C. F. Le; Y. M. Li, "Validation of a quasi-analytical algorithm for highly turbid eutrophic water of Meiliang Bay in Taihu Lake, China," IEEE Trans. Geosci. Remote Sens. **47**(8), 2492–2500 (2009).
43. X. Hou, L. Feng, H. Duan, X. Chen, D. Sun, and K. Shi, "Fifteen-year monitoring of the turbidity dynamics in large lakes and reservoirs in the middle and lower basin of the Yangtze River, China," Remote Sens. Environ. **190**, 107–121 (2017).
44. C. Huang, H. Yang, A. X. Zhu, M. Zhang, H. Lü, T. Huang, J. Zou, and Y. Li, "Evaluation of the Geostationary Ocean Color Imager (GOCI) to monitor the dynamic characteristics of suspension sediment in Taihu Lake," Int. J. Remote Sens. **36**(15), 3859–3874 (2015).
45. Y. Zhang, S. Lin, J. Liu, X. Qian, and Y. Ge, "Time-series MODIS image-based retrieval and distribution analysis of total suspended matter concentrations in Lake Taihu (China)," Int. J. Environ. Res. Public Health **7**(9), 3545–3560 (2010).
46. W. Zhou, S. Wang, Y. Zhou, and A. Troy, "Mapping the concentrations of total suspended matter in Lake Taihu, China, using Landsat□5 TM data," Int. J. Remote Sens. **27**(6), 1177–1191 (2006).
47. Z. Mao, J. Chen, D. Pan, B. Tao, and Q. Zhu, "A regional remote sensing algorithm for total suspended matter in the East China Sea," Remote Sens. Environ. **124**, 819–831 (2012).
48. M. Zhang, J. Tang, Q. Dong, Q. T. Song, and J. Ding, "Retrieval of total suspended matter concentration in the Yellow and East China Seas from MODIS imagery," Remote Sens. Environ. **114**(2), 392–403 (2010).
49. are E. Siswanto, J. Tang, H. Yamaguchi, Y.-H. Ahn, J. Ishizaka, S. Yoo, S.-W. Kim, Y. Kiyomoto, K. Yamada, C. Chiang, and H. Kawamura, "Empirical ocean-color algorithms to retrieve chlorophyll-, total suspended matter, and colored dissolved organic matter absorption coefficient in the Yellow and East China Seas," J. Oceanogr. **67**(5), 627–650 (2011).
50. J. H. Ryu, H. J. Han, S. Cho, Y. J. Park, and Y. H. Ahn, "Overview of geostationary ocean color imager (GOCI) and GOCI data processing system (GDPS)," Ocean Sci. J. **47**(3), 223–233 (2012).
51. D. Doxaran, N. Lamquin, Y. J. Park, C. Mazeran, J. H. Ryu, M. Wang, and A. Poteau, "Retrieval of the seawater reflectance for suspended solids monitoring in the East China Sea using MODIS, MERIS and GOCI satellite data," Remote Sens. Environ. **146**, 36–48 (2014).